AGU PUBLICATIONS

JGR

Journal of Geophysical Research: Oceans

RESEARCH ARTICLE

10.1002/2016JC012170

Key Points:
- A new reliable early warning tsunami detection algorithm has been developed
- A new reliable statistical methodology to test tsunami detection algorithms has been developed
- The algorithm has been installed onboard abyssal observatories and tested in open ocean campaigns

Supporting Information:
- Supporting Information S1

Correspondence to:
F. Chierici,
chierici@ira.inaf.it

Citation:
Chierici, F., D. Embriaco, and L. Pignagnoli (2017), A new real-time tsunami detection algorithm, *J. Geophys. Res. Oceans*, *122*, doi:10.1002/2016JC012170.

Received 19 AUG 2016
Accepted 14 DEC 2016
Accepted article online 27 DEC 2016

A new real-time tsunami detection algorithm

Francesco Chierici [1,2,3], Davide Embriaco [2], and Luca Pignagnoli [2]

[1]Istituto di Radioastronomia-Istituto Nazionale di Astrofisica, Bologna, Italy, [2]Istituto Nazionale di Geofisica e Vulcanologia, Roma, Italy, [3]Istituto di Scienze Marine-Consiglio Nazionale delle Ricerche, Bologna, Italy

Abstract Real-time tsunami detection algorithms play a key role in any Tsunami Early Warning System. We have developed a new algorithm for tsunami detection based on the real-time tide removal and real-time band-pass filtering of seabed pressure recordings. The algorithm greatly increases the tsunami detection probability, shortens the detection delay and enhances detection reliability with respect to the most widely used tsunami detection algorithm, while containing the computational cost. The algorithm is designed to be used also in autonomous early warning systems with a set of input parameters and procedures which can be reconfigured in real time. We have also developed a methodology based on Monte Carlo simulations to test the tsunami detection algorithms. The algorithm performance is estimated by defining and evaluating statistical parameters, namely the detection probability, the detection delay, which are functions of the tsunami amplitude and wavelength, and the occurring rate of false alarms. Pressure data sets acquired by Bottom Pressure Recorders in different locations and environmental conditions have been used in order to consider real working scenarios in the test. We also present an application of the algorithm to the tsunami event which occurred at Haida Gwaii on 28 October 2012 using data recorded by the Bullseye underwater node of Ocean Networks Canada. The algorithm successfully ran for test purpose in year-long missions onboard abyssal observatories, deployed in the Gulf of Cadiz and in the Western Ionian Sea.

1. Introduction

Tsunami Early Warnings are of paramount importance for hazard mitigation. At present, the warning procedure for earthquake-generated tsunamis can be summarized as follows: after a shallow submarine earthquake exceeding a given magnitude, the earthquake parameters and the output of tsunami propagation models are used to issue a warning which is successively confirmed or cleared using sea level measurements. The sea level measurements are needed for a timely validation of the warning since not all large earthquakes actually generate tsunamis, and the issuing of false alarms is quite common. For this reason, the avoidance of false alarms is a major concern for any Tsunami Warning System. Presently, the only effective way to tackle this problem is to minimize the elapsed time between the warning and its cancellation or confirmation and as stated by *Sanderson* [2008]: "the best way to confirm that a tsunami was generated is with ocean-Bottom Pressure Recorders (BPRs) which can spot a tsunami wave passing overhead, or tide gauges that spot wave action on shore." As the tsunami waves travel faster in deep water, the fastest warning validation is achieved detecting the tsunami wave in the open sea with BPRs equipped with real-time tsunami detection algorithms. Effective real-time tsunami detection algorithms are a fundamental tool to perform an early and reliable detection of tsunami waves. In order to a obtain improved and reliable tsunami detection in near source conditions (i.e., with short travel time of tsunamis), which is a common situation for the Mediterranean, Japan (Fukushima, 2011) and the Pacific coasts of Canada and the United States of America, we have developed a new real-time Tsunami Detection Algorithm (TDA), within the framework of the NEAREST EC project (NEAR shore sourcES of Tsunamis: towards an early warning system, http://nearest.bo.ismar.cnr.it/), during 2006–2007.

The TDA, in real time, removes the tidal components of sea level, which are modeled using HAMELS (Harmonics Analysis MEthod of Least Squares) [*Foreman*, 1977; *Pawlowicz et al*., 2002] from the bottom pressure record. The detided bottom pressure signal is then band-pass filtered in real time to obtain the residual signal in the tsunami frequency band [*Chierici et al*., 2007, 2008]. Other periodic components can be removed, where required, using spectral analysis.

The strong reduction in the dynamic range of the time series (up to two orders of magnitude) achievable by removing tidal and other periodic components along with the filtering of signals outside the tsunami

frequency band, allows much more accurate, quick, and reliable tsunami detection (less than 1 cm wave amplitude and near to the theoretical noise limit of 0.23 cm of equivalent water estimated by Zielinski and Saxena, *Zielinski and Saxena* [1983]). The TDA has been installed and has successfully operated onboard the stand-alone GEOSTAR multidisciplinary abyssal observatory (GEophysical and Oceanographic STation for Abyssal Research) during two missions in the Gulf of Cadiz at a depth of about 3200 m from July 2007 to August 2008 and from November 2009 to July 2010 (http://www.moist.it/sites/iberian_margin/1) as a task of the EC NEAREST project and of the EC ESONET-NoE (European Seas Observatory NETwork-of Excellence). The TDA has been also installed and tested using the NEMO-SN1 cabled abyssal observatory (NEutrino Mediterranean Observatory- Submarine Network 1) offshore near Catania (Eastern Sicily), at a depth of about 2100 m during a mission from June 2012 to June 2013 [*Chierici et al*., 2012; *Favali et al*., 2013; *Monna et al*., 2014; *Giovanetti et al*., 2016]. The Gulf of Cadiz and the Western Ionian are nodes of the EMSO research infrastructure (European Multidisciplinary Seafloor and water-column Observatory, http://www.emso-eu.org).

A reliable estimation of algorithm performance is an important task when evaluating the effectiveness of a tsunami detection procedure. In order to evaluate and compare the performance of various real-time tsunami detection algorithms, we have developed a benchmark procedure. For this purpose, we have defined a simple set of statistical parameters, which we believe to be meaningful for characterizing the algorithms, i.e., the tsunami detection probability and the detection delay, which describe the algorithm performance as a function of amplitude and wavelength of tsunami waves, and the rate of false alarms. Clearly, any statistical estimation of these parameters will also be useful for adapting an algorithm configuration to the installation site characteristics and will help in optimizing tsunami detection procedures. The benchmark, which is based on the Monte Carlo method [*Metropolis and Ulam*, 1949], randomly superimposes synthetic tsunamis to real bottom pressure records to estimate the ability of the algorithms in detecting tsunamis.

2. Scientific Background

Starting from the pioneering works of Filloux [*Filloux*, 1980, 1982, 1983] and *Zielinski and Saxena* [1983], the use of BPRs for tsunami detection and warning in deep ocean environments has shown significant developments over the past few decades. BPRs are basic components of all state-of-the-art Tsunami Early Warning Systems (TEWSs) presently in operation such as the DART (Deep Ocean Assessment and Reporting of Tsunami) [*Milburn et al*., 1996; *Gonzalez et al*., 1998; *Meinig et al*., 2005; *Titov et al*., 2005], the Japanese DONET (Dense Ocean Network system for Earthquakes and Tsunamis, http://www.jamstec.go.jp/donet/e/index.html), and the European prototype developed in the EC project NEAREST.

Sea level data can be easily recovered from the bottom pressure time series acquired by BPRs allowing direct measurement of sea level variations and in particular of tsunami waves. Concerning the early detection of tsunamis, a key role is played by the real-time tsunami detection algorithms which process the bottom pressure data acquired by the BPRs and the sea level data acquired by tide gauges to recognize the tsunami parent signals exceeding a given hazardous threshold.

Currently, the most widely used algorithm is that proposed by *Mofjeld* [1997] within the framework of the DART System. The success of the Mofjeld algorithm is due to its effectiveness and to its very low computational cost and ease of implementation. This algorithm is based on a match between a cubic linear prediction of the expected bottom pressure value, obtained using the past 3 h record of pressure data, and the actual measured pressure value; if the difference between the expected and measured values exceeds an assigned threshold then tsunami detection is declared. This algorithm has also been applied to tide gauges in shallow water environments with slight modification of algorithm parameters [*Beltrami and De Girolamo*, 2006].

As shown by *Beltrami* [2008] a pure predictive algorithm, such as that proposed by Mofjeld, fails in reducing the high frequency component of environmental noise, which is also the most energetic one [*Zielinski and Saxena*, 1983]. Here the term high frequency refers to a signal whose frequency is higher than 0.083 Hz, which is the upper end of the tsunami frequency band. Contributions to such a noise may stem from different sources, like sea state and primary and secondary microseisms [e.g., *Gualtieri et al*., 2015; *Tian et al*. 2015]. The deployment of seafloor BPRs at depth can help in filtering the so called single-frequency noise component due to linearly generated pressure fluctuation following a single surface train, because this noise is exponentially attenuated by water column height [*Lamb*, 1932]. On the contrary, the contribution

due to the double-frequency component generated from non linear interaction between opposing surface wave trains exhibits little depth dependence [*Kibblewhite and Ewans*, 1985; *Traer and Gerstoft*, 2014; *Kadri and Akylas*, 2016]. The effective removal of high frequency noise from the bottom pressure time series is a fundamental task for any tsunami detection algorithm.

In addition to the Newton linear prediction adopted by Mofjeld, many different techniques have been proposed to implement effective real-time tsunami detection algorithms. All the algorithms proposed can be divided into two main categories: (a) slope discriminating and (b) amplitude discriminating. Slope discriminating algorithms take advantage of the different slopes induced in the sea level signal by the action of tides and short wavelength sea waves compared to that of tsunami waves. This class of algorithms involves waiting for at least one sample after the first quarter period of the tsunami wave, before triggering a potential event in order to be sure that the perturbation falls within the typical tsunami frequency range and when, at the same time, an amplitude threshold has been exceeded. *McGehee and McKinney* [1997] proposed a detection algorithm based on matching successive mean slopes of the bottom pressure time series. This algorithm has been tested using the data set of the 4 October 1994 Shikotan event [*Tanioka et al*., 1995].

On the other hand, amplitude discriminating algorithms are based on the estimation of a threshold of wave height in the typical tsunami frequency range which, if exceeded, triggers the detection of the potential tsunami. Such algorithms are very timely and effective if the pressure disturbance greatly exceeds the given threshold. An example of such algorithms is the Mofjeld tsunami detection algorithm adopted by the DART network.

Some authors have suggested the application of neural network techniques to tsunami detection like *Beltrami* [2008], which has proposed a real-time tsunami detection algorithm based on an Artificial Neural Network.

Wavelet transforms have also been used in postprocessing for the implementation of tsunami detection algorithms and a first attempt at the automatic detection of tsunami waves generated by landslides was made [*Panizzo et al*., 2002, 2005].

Other attempts have been made to take into account tidal parameters in the real-time tsunami detection procedure. Empirical Orthogonal Function (EOF) analysis was applied by Tolkova [*Tolkova*, 2010] to 3 day long pressure record segment in order to remove the 1 day trend of the tide and to enhance the detection of tsunami signals in the pressure time series with gaps in the data acquisition. Successively, *Bressan and Tinti* [2011] proposed estimating the long-term average slope induced by the tide signal within the sea level record using first-order polynomial fitting, and then comparing this slope to the short-term average slope of the time series. In a successive paper, this technique was applied to the March 2011 Tohoku tsunami tide gauges data [*Bressan and Tinti*, 2012].

All the quoted algorithms, while delivering average good performances, show some critical aspects: amplitude discriminating prediction algorithms, like the ones developed by Mofjeld and Beltrami, suffer from a memory effect, affecting the characterization of the tsunami waves or, alternatively, the detection delay [*Beltrami and Di Risio*, 2011]. Slope discriminating algorithms, like the one developed by *Bressan and Tinti* [2011] show some unsuccessful detections, at least when small amplitude tsunamis are concerned. In conclusion, as reported in *Rabinovich and Eblé* [2015]: "the corresponding algorithms struggle to balance suppression of tides with retention of the tsunami; either leaving a few percent of tidal energy [*Di Risio and Beltrami*, 2014], or distorting the tsunami signal."

In order to evaluate the effectiveness of the tsunami detection algorithms, several approaches have been proposed in the literature [*Beltrami and Di Risio*, 2011; *Bressan and Tinti*, 2011]. These approaches, however, do not provide a statistical estimation of the performance of tsunami detection algorithms.

In the following, we describe the TDA, the benchmark procedure and the parameters used to quantify algorithm performance (sections 3 and 4 respectively). Finally, section 5 discusses the result of tests using various bottom pressure data sets and a comparison between the TDA and the Mofjeld algorithm used by DART, which is taken as a benchmark, since it is widely used in Tsunami Warning Systems.

3. The Tsunami Detection Algorithm (TDA)

The TDA is composed of a cascade of filters (Figure 1): the filtering cascade is a series of procedures including tide removal, spike removal, and real-time band-pass filtering in order to remove the effects of tides, spikes and high and low frequency noise.

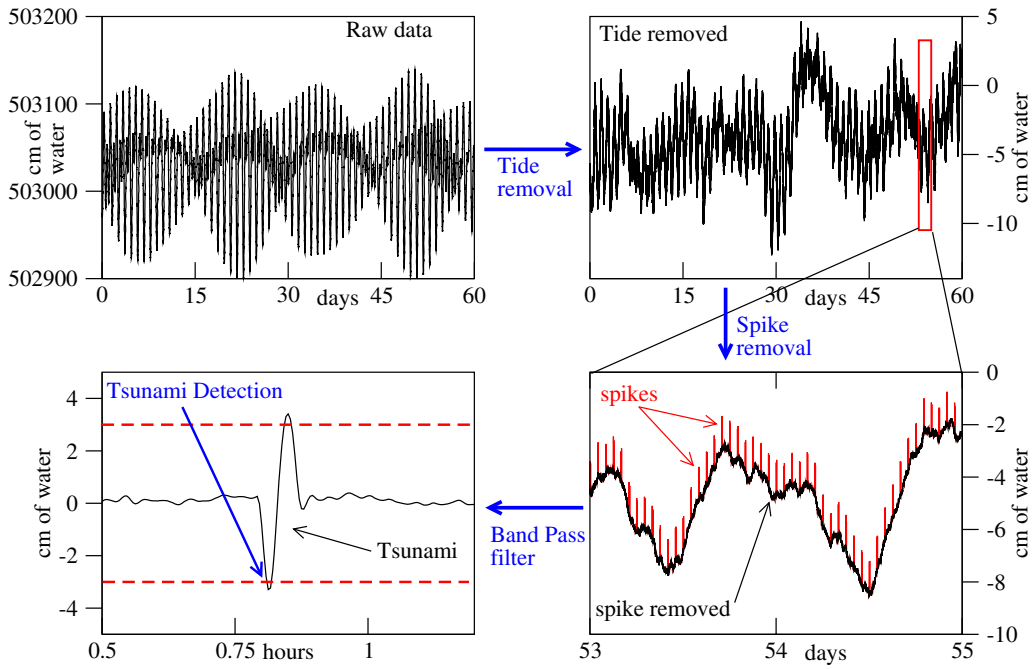

Figure 1. The real-time tsunami detection algorithm scheme. The dynamic range of the signal (raw pressure data on top left) is reduced from about 200 cm of equivalent water to about 1 cm by the filtering chain: (top right) tide removal, (bottom right) spike removal, and (bottom left) band-pass filter. A tsunami is detected in the residual signal when it exceeds the threshold (bottom left, dashed red line at ±3 cm). Note the different time scale in top and bottom plots: 60 days in the top plots, 2 days in the bottom right plot, 45 min in the bottom left plot. Raw data are from DART buoy D165 (see Tables 1, 2 and text for details), tsunami in the bottom left plot is synthetically generated and added to the data as an example.

Tides are modeled using harmonic summation [*Jay and Flinchem*, 1999; *Pawlowicz et al.*, 2002]:

$$y(t)=a_0+\sum_{i=1}^{i=N} a_i\cos\left(\omega_i t+\varphi_i\right) \tag{1}$$

where a_0 is the mean sea level value, a_i are the amplitudes of the N periodic components of the sea level signal, $\omega_i/2\pi$ and φ_i are their frequencies and phases, respectively, and t is the time.

The tide removal procedure requires the recovery of periodic parameters at the installation site, such as tide and basin normal mode coefficients. For this reason, the algorithm needs the acquisition of an appropriate amount of sea level data before it can fully express its ability in detecting parent tsunami signals. The minimum number of samples needed to perform the Fourier harmonic analysis of a particular periodic component can be obtained using the Rayleigh criterion. This criterion establishes whether a tidal harmonic can be resolved and included in the analysis, depending on its frequency, its vicinity to other harmonics and on the sampling rate and length of the time series from which the periodic components are extracted [*Foreman*, 1977]. Nevertheless using HAMELS method, the first eight tide coefficients can be recovered over several days, with 3 months of BPR data 35 tide coefficients can be computed and used in the tide removal procedure. In fact, the use of least square approach in harmonic analysis allows less stringent constrains in the selection of the tidal coefficients, based on the matrix condition number. Other periodic nontidal components, such as basin resonances, can be identified and recovered by performing a power spectrum analysis of the bottom pressure signal. Due to unaccounted effects in the sea level record [*Pugh*, 1982; *Foreman*, 1977] the tide coefficients must be periodically recomputed to maintain the accuracy of the tide removal procedure. As mentioned above, removal of the predicted tide level strongly reduces the dynamic range of the BPR data greatly improving the reliability of tsunami detection, for instance, from about 2 m of equivalent water height to only a few cm in open ocean, as in the examples shown below. Spike removal eliminates noise due to external factors. Such disturbances can, for example, derive from acoustic transducers used for submarine communication, which may cause large sudden variations in pressure data if not properly shielded, or from short electronic glitches. Classical spike removal techniques, such as linear or median

filters, should not be applied in tsunami detection procedures because they produce a slight damping of the amplitude of very short period (2–3 min) tsunami parent signals. To overcome this problem we have included a logical filter which works by rejecting a sample S_i at time t_i and substituting the value of the external disturbance with a mean value between S_{i-1} and S_{i+1} when:

1. S_i is far from the median value M of a small set of data (for instance, the last 5–10 samples) i.e., if the module of the difference $|(S_i - M)| > V$, where V is an assigned value.
2. The modules of the differences $|(S_{i-1} - M)| < V$ and $|(S_{i+1} - M)| < V$, where S_{i-1} and S_{i+1} are the values of preceding and successive samples.

The decision of rejecting a sample or not is hence taken by comparing the last acquired sample with the last-but-one and the last-but-two samples thus avoiding a wrong rejection in the case of signals induced by steep tsunami waves [*Menold et al.*, 1999]. This filter delays the tsunami detection procedure by one sampling period (typically 15 s) which is acceptable even for very Early Tsunami Warning purposes.

Despiked data are then processed by the band-pass filtering routine. The standard formula of a generic discrete digital Finite Impulse Response (FIR) band-pass filter is given by:

$$y_n = \sum_{i=-N}^{i=+N} c_i S_{n-i} \tag{2}$$

where S_i and c_i are the ith acquired sample of the time series and the ith filter coefficient, respectively, N is the filter order and y_n is the filtered sample.

Usually the filter (2) is applied in postprocessing at sample n of a time series that is comprised between sample $n - N$ and sample $n + N$. This procedure causes a critical lag of N samples if applied to a real-time algorithm. To overcome this problem, a synthetic record of N samples can be used, instead of waiting for the availability of the data segment that follows sample n. *Wah and Qian* [2002] presented a brief review of the approaches used to generate the synthetic record: (a) flat extension, (b) mirror extension, (c) wrap around, and (d) zero extension. The wrap around and zero extension methods fail when a trend is present in the time series, because in this case they introduce a sharp jump in the data record which can result in false detections. For this reason, we only tested the mirror and flat extension approaches by using real data sets and we obtained similar results. In the end, we chose the mirror extension solution because it does not underestimate the pressure signal avoiding possible detection failure.

We can rewrite equation (2) using the mirror extension obtaining:

$$y_n = c_0 S_n + 2\sum_{i=1}^{i=N} c_i S_{n-i} \tag{3}$$

The data, band-passed within the typical tsunami frequency band, are then matched against the warning threshold in order to detect a parent tsunami signal i.e.:

$$\text{if } |y_n| \geq V_T \text{ then issue a warning, else continue} \tag{4}$$

V_T is the assigned threshold amplitude.

The shape, frequency band, and the order of the band-pass filter can be selected on the basis of the particular environmental conditions at the location of the tsunami detector to optimize detection performance.

The algorithms were implemented in such a way that all its parameters, i.e., the band-pass filter, the threshold and the number of points to be used in the spike removal routine, the phase and amplitude of tide and basin coefficients and the threshold for the tsunami detection can be real-time configured or changed during the mission. Moreover, the algorithm was designed as a modular filtering cascade, into which new routines can be easily integrated and where any module can be independently activated. Particular attention was devoted to algorithm optimization to achieve low computational requirements in the case of battery-powered stand-alone tsunami detectors. For the TDA configuration tested in the field, i.e., 7 points spike removal median filter, 35 coefficients tide removal, and 4000 points band-pass filter, the algorithm requires less than 4200 floating point operations for each iteration.

Figure 2 reports the algorithm flow chart.

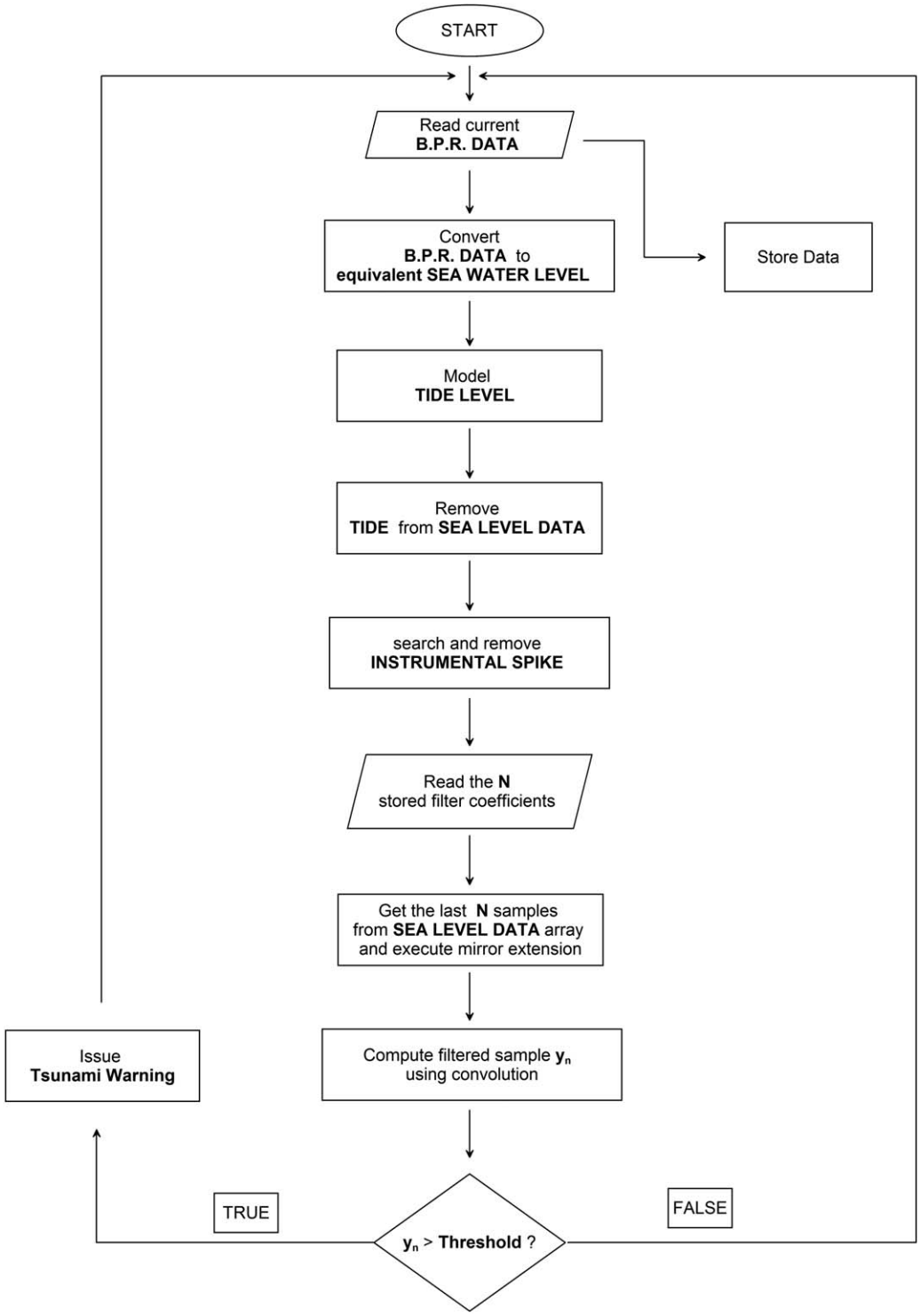

Figure 2. Flow chart of the new tsunami detection algorithm.

4. Procedure for the Assessment of the Performance of Tsunami Detection Algorithms

The validity and robustness of any tsunami detection algorithm can be enhanced by maximizing the detection probability, minimizing the detection delay and lowering the false-alarm rate, over a given time

interval. For this reason, the setting up of a procedure to measure the ability of an algorithm in detecting tsunami signals and tuning its efficiency is desirable. A quantitative characterization of the performance of an algorithm can be obtained by accurately estimating the probability and the rapidity of detection of the parent tsunami signals as well as the rate of false alarms. These three parameters should be evaluated for both tsunami polarities, in the whole tsunami frequency band and for a wide range of tsunami amplitudes and shapes and possibly under a variety of environmental conditions. The statistical evaluation of these parameters will help in tuning and optimizing the algorithm configuration under those given conditions. To this end, the use of real data sets, acquired in different locations and environmental conditions, suitably characterized, is important for any reliable evaluation of algorithm performance under operating conditions.

These three statistically valuable indicators are defined below, and a procedure is described for their statistical estimation using Monte Carlo simulations.

We define the tsunami detection probability P as the probability that a given tsunami wave is detected by the algorithm and the tsunami detection delay D as the time lag between the detection of the tsunami and the arrival of the very first part of the wave at the detector position.

The false-alarm rate F is defined as the number of detections per unit of time, if no tsunami waves exceeding the assigned amplitude threshold are present in the bottom pressure record. The false-alarm rate defines the number of false alarms we can expect on average, for example in one year, in that particular place, by using that particular detection algorithm with that configuration and that choice of detection threshold value.

In order to provide a valid estimation of the parameters P, D, and F we set up a procedure which can be used with any real-time tsunami detection algorithm. As a first step suitable data sets must be selected to be used as a test bed for the procedure, as the algorithm performance may depend on the installation site characteristics and seasonal variations.

We chose three different data sets, each about 1 year long: the recordings of DART D165_2001 and D125_2002 stations and of the GEOSTAR-NEAREST_2009 pressure data set (GEOS), acquired over different periods and located in different positions, i.e., in the Central Pacific, near the coast of Alaska and in the Gulf of Cadiz offshore Cabo de Sao Vincente, in the NE Atlantic Ocean respectively (see Figure 3, Table 1, and supporting information Figures S1, S6, S11, for details and references).

Each bottom pressure record can be characterized by a power spectrum (see Figure 4), standard deviation and minimum and maximum value of the mean sea level variation (see Table 2 and supporting information Figures S1, S6, S11) in order to allow a comparison among different records and to facilitate the interpretation of the statistical results (see Table 2).

Synthetic tsunami waves were superimposed on these data sets, using the Monte Carlo method in order to obtain the time series to feed the tsunami detection algorithms and to statistically evaluate their performance. The superimposed tsunamis were generated with amplitude and period randomly distributed; in our simulations amplitudes between zero and 5 cm and periods between 120 s and 2 h were used allowing both positive and negative polarities in order to verify possible phase dependencies of the triggering mechanism. The starting time for each tsunami was randomly chosen within the data sets. Between two injected tsunamis a temporal window of several hours was interposed, ensuring that the initial part of a tsunami was far enough from the end of any previous one to avoid correlation effects in the simulation. For each synthetic tsunami added to the data sets, the evaluation procedure verifies whether or not the tsunami was detected by the algorithm and the possible detection delay with respect to its starting time. The procedure was repeated a suitable number of times to obtain a statistically meaningful sample size for the tsunami population. The randomly chosen starting time of the tsunamis along the time series, ensured that the population of synthetic waves used to probe the algorithm represented a good sample, in a statistical sense, of tsunami events with those particular features, i.e., amplitudes, polarity, and periods. In other words, this Monte Carlo based benchmark performs many times and for different tsunami amplitudes and polarities a benchmark similar to the test procedure implemented by *Beltrami* [2008], which superposed sinusoidal synthetic tsunami signals to a synthetic tide signal summed to white noise. In our procedure the white noise is substituted by real environmental noise and the synthetic tide is substituted by real tides.

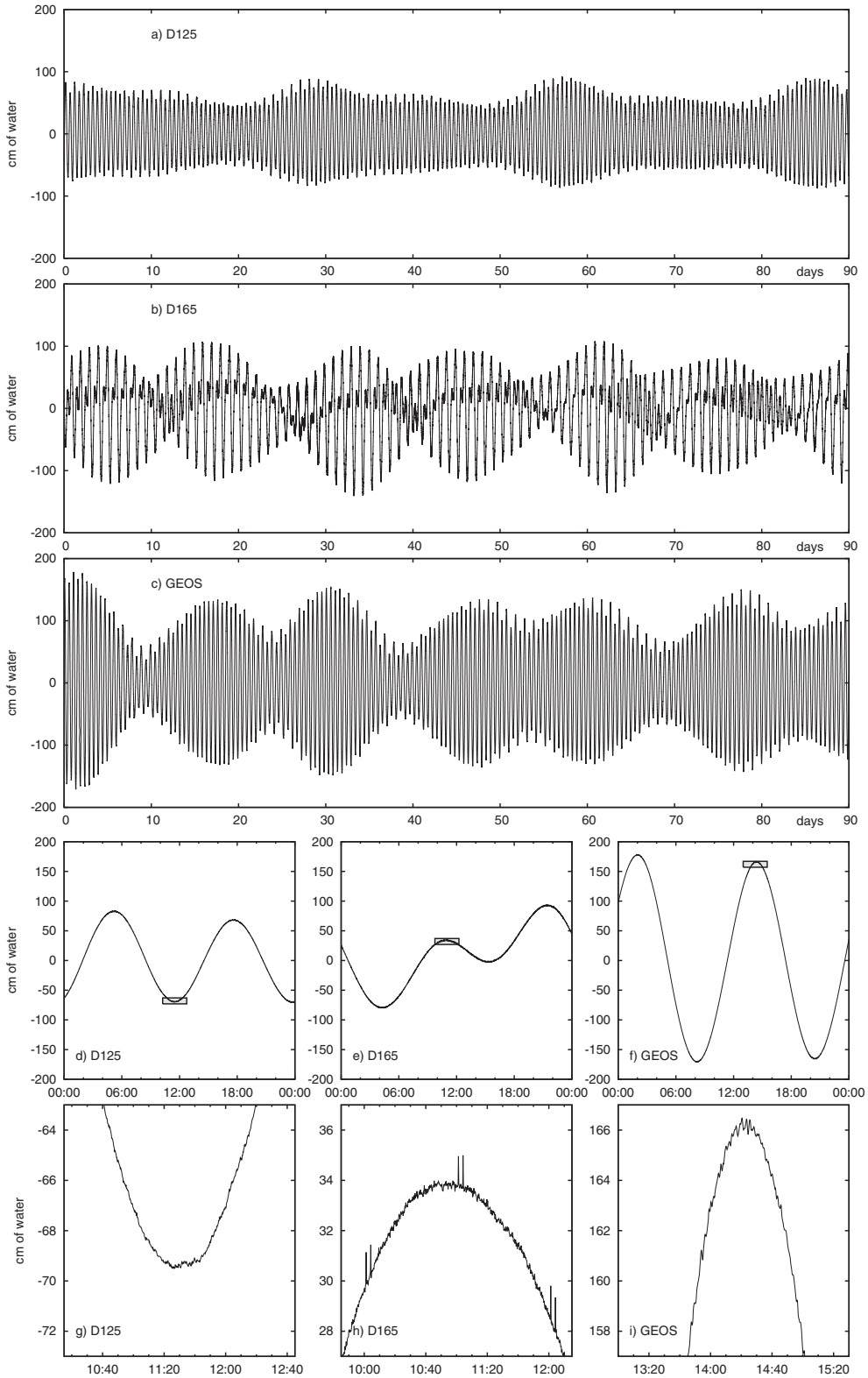

Figure 3. Insets (a, b, c) show examples of the data sets used in the simulations, i.e., D125, D165 and GEOS, respectively. The pressure variation with respect to the mean sea level is measured in cm of equivalent water (1 cm of equivalent water ≈100 Pascal). Insets (d, e, f) show a zoom of one day of data namely the second day of each data set. The gray rectangular areas boxes mark the 2.5 h data intervals which are showed in details in inset (g, h, and i), respectively. Inset h reports hourly spikes, of amplitude about 1 cm, due to unshielded data transmission of the DART bottom module acoustic modem.

Table 1. BPR Data Set Used in the Simulation Tests[a]

Data Source	Location	Latitude (N)	Longitude (W)	Time Period	Data Set
D125_2002-ed.dat	Equatorial Pacific Ocean at 4500 m depth	8.488700	125.010000	From 15 Jan 2002 to 27 Jan 2003	D125
D165_2001-ed.dat	South of Dutch Harbor, AK at 4936 m depth	50.440600	165.038900	From 1 Jun 2001 to 17 Jun 2002	D165
GEOS data set	North-East Atlantic Ocean, Gulf of Cadiz at 3264 m depth	36.352917	9.518245	From 10 Nov 2009 to 10 Jul 2010	GEOS

[a]D125 and D165 were obtained from National Oceanic and Atmospheric Administration (2005): Deep-Ocean Assessment and Reporting of Tsunamis (DART(R)). National Geophysical Data Center, NOAA. doi:10.7289/V5F18WNS [access date: 20/11/2015]. GEOS data set is available fromhttp://www.moist.it/sites/iberian_margin/1/LIDO1/pressure_gauge/19.

Statistics were extracted by grouping together the output of the algorithm with respect to tsunamis of similar amplitudes and periods. An estimation of the detection probability P was computed by dividing the number of detected tsunamis by the number of generated tsunamis within the given interval of amplitudes and periods. The detection delay D was estimated as the mean value of the measured detection delays within a given interval of tsunami amplitudes and periods. Finally, the false-alarm rate F was estimated by counting the number of false detections divided by the duration of the time series. To estimate F, raw data are postprocessed by applying a band-pass filter in the tsunami frequency band. The filtered residual is then analyzed to identify, mark and count any potential tsunami parent signal exceeding the prescribed threshold which would produce a true detection: any other detection which do not correspond to the identified ones is considered false. In conclusion, the described method comprises the setting up of a statistical procedure to estimate the performance of any tsunami detection algorithm.

5. Results and Discussion

The TDA was developed in particular for operation in areas with short time delays between the occurrence of an earthquake and the arrival of the first tsunami wave, for this reason, particular attention was devoted to designing an algorithm able to detect a tsunami parent signal as soon as it exceeds a fixed threshold.

In order to evaluate algorithm performance, we applied the test procedure described in the previous section to the TDA and, as a reference, to the Mofjeld algorithm which is a very effective algorithm and the most widely used and tested.

For the TDA set up, we used a tide removal with 35 tide coefficients, a 7 points median and 1 cm threshold for spikes removal, and a order 4000 Hann window band-pass (120–7200 s) filter. This is the same configuration used during the NEAREST project onboard the GEOSTAR multidisciplinary stand-alone abyssal observatory and for the NEMO-SN1 cabled multidisciplinary abyssal observatory. For the Mofjeld set up, we chose three 10 min averages over the 3 h preceding the last acquired point, to compute the coefficient of the cubic polynomial used for tide prediction [*Mofjeld*, 1997]. The Tsunami detection threshold has been chosen at 3 cm.

For benchmarking, three data sets were used, two of which by courtesy of DART, acquired in the Pacific, South of Dutch Harbor, AK, and Equatorial Pacific Ocean and the GEOSTAR-NEAREST data set acquired in the North East Atlantic Ocean (details and references in Tables 1 and 2). We tested the two algorithms by running the Monte Carlo simulation for each data set. We performed the simulation by injecting tsunamis with periods ranging from 120 to 7200 s and amplitudes from -5 to 5 cm. To perform the Monte Carlo simulation, we randomly inject about 10^6 synthetic tsunamis, uniformly distributed in amplitude, period, polarity, and position over each bottom pressure record because we are interested in exploring the whole tsunami's parameter space and not a particular range of parameter values. The results of the benchmark procedure are presented as 80×80 cells maps of the parameter space, each cell containing 150 synthetic tsunamis on average and at least 100 tsunamis. In this way each cell of the map contains a suitable number of events to allow the computation of a reliable statistics.

We used a sine wave tsunami form as a good approximation of tsunamis in the open ocean [*Bryant*, 2014], the benchmark data sets being acquired in deep water. Some examples of superimposed tsunamis to the

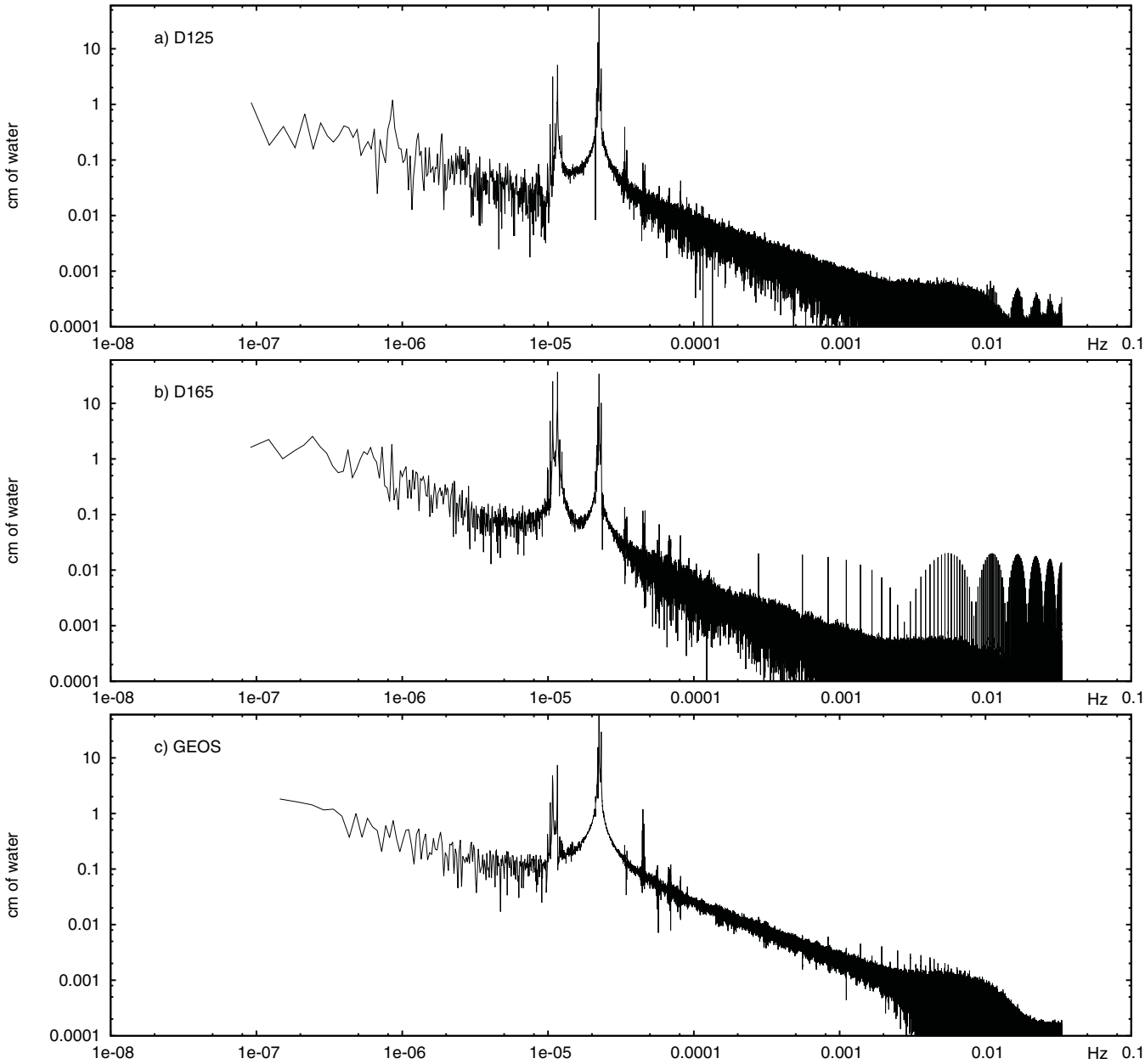

Figure 4. Amplitude spectra of D125, D165, and GEOS. In inset (b) the effect due to the hourly spikes which are present in the time series D165 is clearly visible.

Table 2. Minimum and Maximum Variation of the Mean Sea Level and the Standard Deviation Values for Each Data Set Used to Test the Algorithms Performance Are Shown[a]

Data Set	Min Sea Level	Max Sea Level	Standard Deviation	Parent Tsunami Signals Over 3 cm	Notes
D125	−86.85 cm	97.06 cm	43.74 cm	0	
D165	−143.3 cm	118.5 cm	47.57 cm	0	Hourly spikes (amplitudes of about 1 cm)
GEOS	−182 cm	189.8 cm	75.94 cm	0	

[a]The number of tsunami parent signals occurring in each data set, exceeding the 3 cm threshold is indicated along with particular notes characterizing the data.

real data sets are shown in Figure 5. As pointed out by Masden [*Madsen et al.*, 2008] or by An and Liu [*An and Liu*, 2014], the shape of tsunami waves changes from deep to shallow water and for this reason different waveforms should be chosen to apply our benchmark method to shallow water sites [see *Tadepally and Synolakis*, 1996] which suggest the use of N shaped

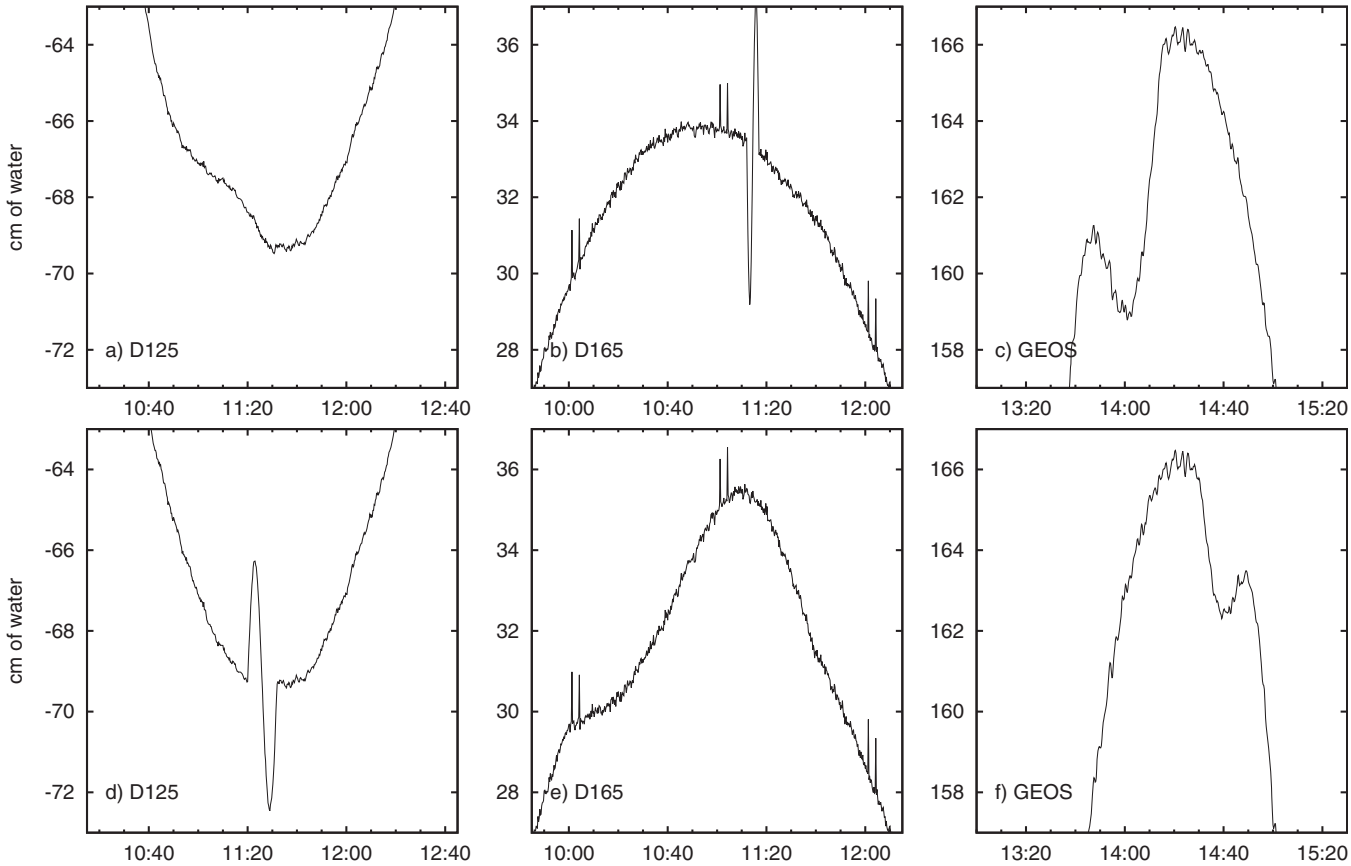

Figure 5. Some examples of synthetic tsunamis generated in the simulation and superimposed to raw data sets. D125 data set: superimposed tsunami in inset (a) period 3600 **s** and amplitude 1cm and in inset (d) 720 s and 3 cm, respectively. D165 data set: superimposed tsunami in inset (b) period 300 s and amplitude 4 cm, in inset (e) 6000 s and 2 cm, respectively. GEOS data set, superimposed in inset (c) tsunami period 2700 s and amplitude 4.5 cm and in inset (f) 1800 s and 2 cm, respectively. Note that the portion of data shown is the same of Figure 3. Data are given in cm of equivalent water.

wave in very shallow water or other authors which suggest solitary waves or bores). Obviously also the TDA configuration should be changed in this case, eventually using a different band-pass filter or a different threshold.

Figure 6 shows the tsunami detection probability maps, both for TDA and Mofjeld algorithms and for each data set considered (D125, D165, GEOS). Each points of the map shows the average detection probability that a wave with that amplitude and period will be detected. For each cell the detection probability P is computed taking the ratio between the number of detected tsunamis and the number of injected tsunamis in each cell: P is represented using a colorimetric scale ranging from 0 (black) to 1 (yellow). In this representation the optimal algorithm output, i.e., detection probability $P = 1$ over the whole tsunami frequency range and for any tsunami amplitude exceeding the fixed threshold, would correspond to two rectangular yellow areas, ending at the detection threshold value, contouring a black one.

The detection probability maps (left column in Figure 6) show the results for the TDA: it produces a map very close to the optimal case over all periods and amplitudes. The output of the Mofjeld algorithm (right column) applied to the same data sets is reported for comparison: as can be seen, tsunamis with long periods are underestimated and tsunamis with period in the range 500–2000 s are overestimated.

The TDA is able to detect most of the tsunamis injected into the records throughout the whole period range and moreover it slightly overestimates tsunami amplitudes within a narrow strip close to the detection threshold value. We point out the importance of evaluating the performance of tsunami detection algorithms with respect to the tsunami period (Figure 6).

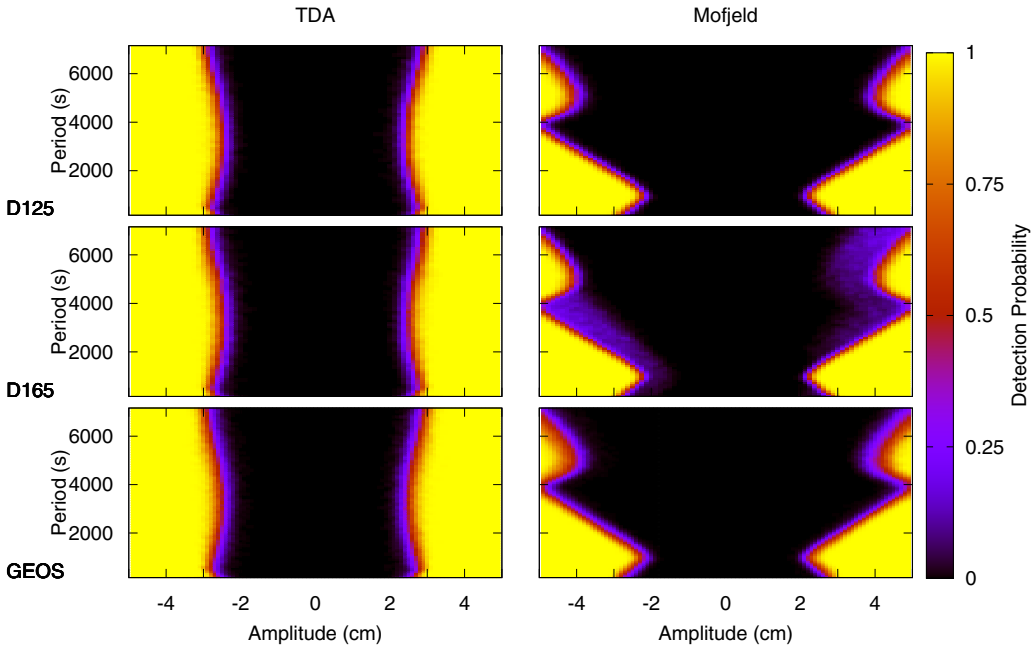

Figure 6. Detection probability *P* as a function of tsunami amplitude and period for the (left) TDA and (right) Mofjeld; the simulations used (from top to bottom) D125, D165, and GEOS data sets; tsunami detection threshold is 3 cm.

The detection delay *D* is an even more important parameter, in particular for tsunami sources located near to coasts, as it measures the rapidity of an algorithm in detecting a tsunami. *D* is computed taking the average value of each tsunami detection delay over a cell. Figure 7 shows the detection delay of TDA (left column) compared with that of the Mofjeld algorithm, both estimated using the Monte Carlo procedure. Here the colorimetric scale spans from black, which means 0 delay, i.e., no delay, to purple which corresponds to a detection delay equal to a very small fraction of the tsunami period, up to 1/4, and to yellow, corresponding to detection delays equal to the tsunami period. White areas correspond to no tsunami detected with

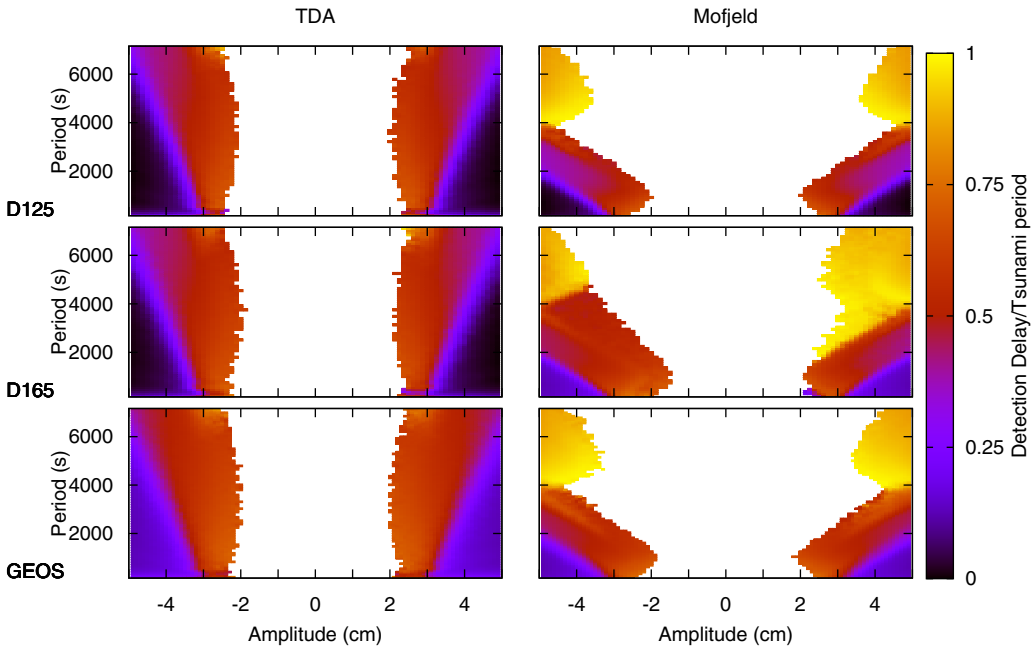

Figure 7. Detection delay as a function of tsunami amplitude and period for the (left) TDA and (right) Mofjeld; the simulations use (from top to bottom) D125, D165, and GEOS data sets; tsunami detection threshold is 3 cm.

that amplitude and period. As shown in Figure 7, the TDA algorithm detects 40% of the tsunamis within the first quarter of their period and the remaining 60% within the first half period with better results for increasing tsunami amplitude and decreasing period length, achieving a very good performance for very early warning.

The Mofjeld algorithm detects 10% of tsunamis within the first quarter of their period, 20% within the first half and 60% within 3/4 of period or more achieving a good performance for distant source tsunamis.

A particular comment pertaining to the performance of the Mofjeld and TDA approaches applied to the D165 data set as shown in Figures 6 and 7 should be made. The D165 record is characterized by the presence of noise from periodic impulses, deriving from acoustic communication from that DART bottom unit to the oceanic buoy which ensures data transmission to land. This noise caused a short-period disturbance in the raw data (one or two samples at 15 s sampling rate) which resulted in a local increase of pressure of the order of 1 cm of equivalent water (see Figure 1, spike removal panel). The effect of this noise on detection probability and detection delay using the Mofjeld algorithm can be seen in D165 data set in Figures 6 and 7 (central plot, on the right). The detection probability map shows a spreading of the low probability contour, which widen the area of the detection probability with respect to the other pressure records. This spreading is due to the presence of the spikes which enhance the detection of tsunami waves of 3–4 cm in amplitude, with periods ranging from about 3000 to 7200 s for positive polarity and with periods from about 1000 to 4000 s for negative polarity tsunamis.

In Figure 7, the average detection delay with the Mofjeld algorithm is about one wave period, for positive polarity in the period range 4000–7200 s and a detection delay slightly more than a half period for negative polarities. The asymmetry with respect to different polarities of the waves is due to the intrinsic asymmetry of the noise in the data set, i.e., such peaks are always "positive."

The spike removal procedure implemented in the TDA efficiently removes the spikes from the pressure data (see Figure 1) producing detection probability and detection delay maps as good as those obtained from the GEOS and D125 records which are not affected by these disturbances.

The tide coefficients used by TDA to obtain the results shown in Figures 6 and 7 were recovered using 6 months' bottom pressure data to predict a further 3 months of tides. The good result obtained suggests a recipe for the timely updating of tide coefficients for that particular detection threshold. The tide coefficients can be exploited for a reliable prediction length up to 50% of the data time span used to compute the coefficients themselves. In general one can say that the lower the detection threshold and the higher the accuracy of the tide prediction required, the shorter the reliable tide prediction length.

The third parameter used to describe the performance of tsunami detection algorithms is the false-alarm rate. The false-alarm rate is estimated by counting the number of tsunamis detected in the raw data records D125, D165, and GEOS where no parent tsunami signals exceeding the prescribed threshold are present (see results in Table 3) and dividing this number by the temporal length of the data set. The rate of false alarms measures the propensity of the algorithm to trigger in the absence of parent tsunami signals exceeding the threshold, thus giving an estimation of the reliability of a warning.

The D165 noisy data set results in a large number of false detections with the Mofjeld algorithm mainly due to the presence of repeated disturbance by the acoustic transmission. The TDA presents no false detection for thresholds of 2 and 3 cm achieving in these simulations a false-alarm rate lower than one false-alarm per year. The Mofjeld algorithm presents one false-alarm per year for the D125 data set while 6 and 2 false-alarms per year are detected using 2 and 3 cm thresholds, respectively, for the D165 data set (see supporting information for D125: Figures S2, S3, S4, S5; for D165: Figures S7, S8, S9, S10; for GEOS: Figures S12, S13, S14, S15).

Table 3. False-Alarm Detection by TDA and Mofjeld Algorithms With the Three Data Sets Considered in the Tests, Using a Threshold of 2 and 3 cm for Tsunami Detection

	TDA		Mofjeld	
Data Set	2 cm	3 cm	2 cm	3cm
D125	0	0	1	1
D165	0	0	6	2
GEOS	0	0	1	1

The use of real bottom pressure time series acquired at depth and the particular choice of sinusoidal waves as a model of the synthetic tsunamis injected in bottom pressure records restrict the validity of our statistical results to deep water environment.

In Figure 8, we show the application of the TDA to a data set which contains a real tsunami event, as acquired

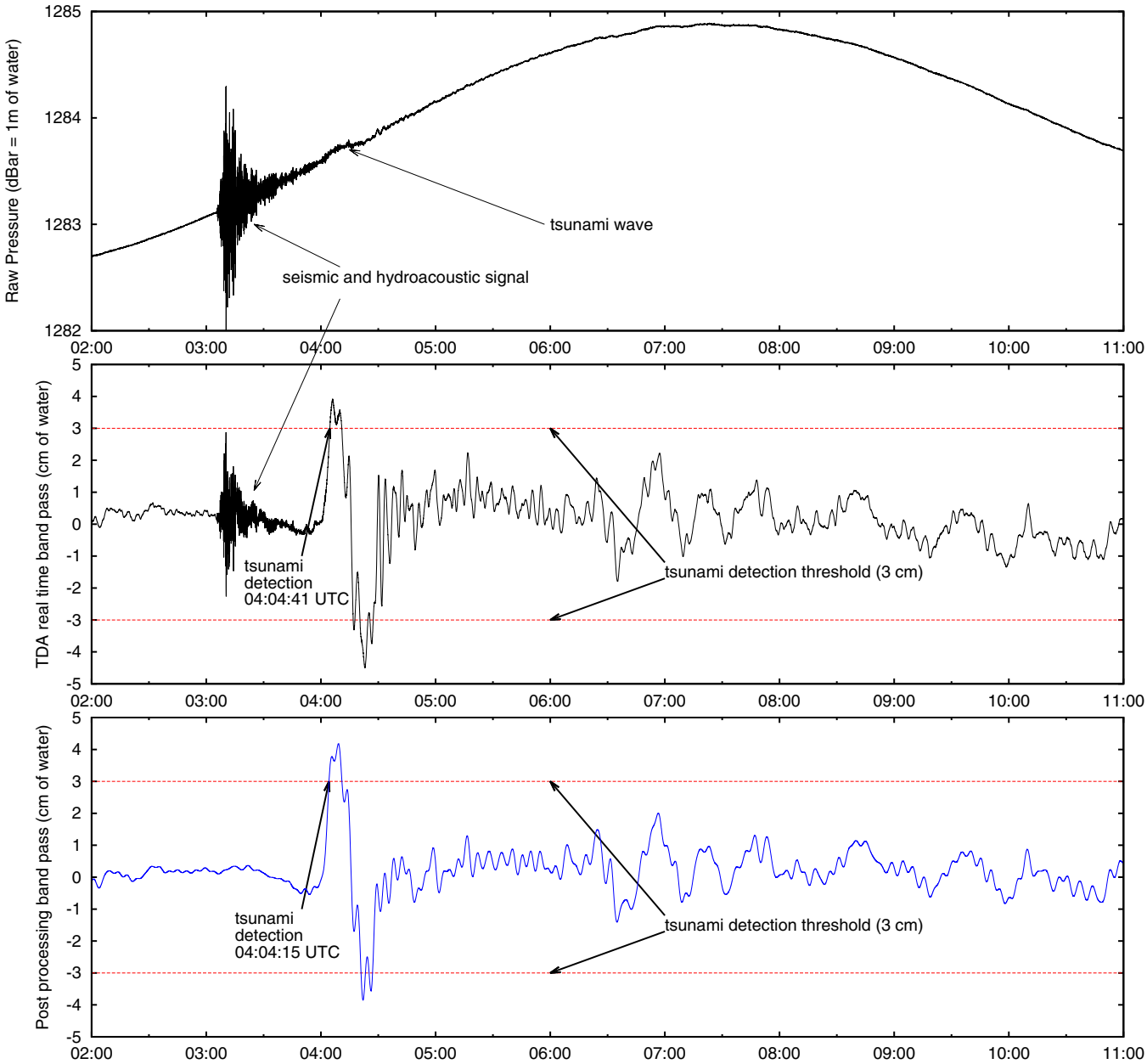

Figure 8. Detection of a real tsunami from pressure data recorded by the ODP 889 BPR of ONC. The pressure sensor is located about 590 km south of the 28 October 2012 (03:04 UTC) Haida Gwaii earthquake (original data from Ocean Networks Canada Data Archive, http://www.oceannetworks.ca, ODP 889 data from 28 October 2011 to 28 October 2012). (top plot) Pressure data (in dbar) sampled at 1 s; (bottom plot) filtered data (in cm of equivalent water) obtained by the real-time TDA algorithm (black line) and comparison with the detection threshold (3 cm, red line). Blue line in bottom panel is the postprocessing (offline) band-pass filter of tide-removed data to highlight tsunami wave features. Note the difference of pressure units in the two plots (1 dbar = 100 cm of equivalent water).

at the Bullseye site of the NEPTUNE observatory of Ocean Networks Canada (ONC). This site is located at Clayoquot Slope, "approximately 20 km landward of the toe of the Cascadia subduction zone" as reported in the ONC website (www.oceannetworks.ca/installations/observatories/northeast-pacific/clayoquot-slope). The site is about 1258 m deep and includes a platform hosting, among many other sensors, the ODP889BPR bottom pressure recorder which acquires data at 1 sample per second. The pressure gauge is a Paroscientific 8B4000-2. The ODP889BPR recorded the Haida-Gwaii tsunamigenic seismic event of 28 October 2012. The tsunami, which reached a run up of about 7 m in several uninhabited inlets of the west coast of Moresby Island and fortunately of smaller amplitudes along the Pacific coasts with a maximum of 0.79 m recorded by a tide gauge in Hawaii, was triggered by a M_w= 7.8 thrust faulting earthquake which occurred

at 03:04 UTC off the Haida Gwaii archipelago. The earthquake hypocenter was localized at 14 km depth, 52.788 N, 132.101 W on the boundary between the Pacific and North America plates [*Cassidy et al*., 2014]. The ODP889BPR is located about 590 km south of the Haida-Gwaii epicenter and was reached less than 2 min after the event by the seismic signal, after less than 7 min by the hydro-acoustic signal generated by the earthquake [*Chierici et al*., 2010; *Abdolali et al*., 2015, *Oliveira and Kadri*, 2016; *Bagheri et al*., 2016] and after 55 min by the tsunami wave (Figure 8, top plot original data). Black line in the middle panel of Figure 8 shows the output of the TDA process performed by the algorithm resulting from the real-time band-pass filtering applied to the detided data. As can be seen, the dynamic range of the residual signal was strongly attenuated, from meters to centimeters of equivalent water, as were the hydro-acoustic and seismic signals. In the real-time application of the TDA, the tsunami amplitude exceeds the detection threshold, here fixed at 3 cm, about 370 s after the very first arrival of the main tsunami wave, hence the TDA detection delay is less than 1/5 of the tsunami period (which is about 31 min). This result shows the excellent performance of the TDA which proves to be particularly suitable for very early warning applications because it is able to detect a small amplitude (in open ocean) tsunami well before its first quarter period.

It is also worth noting that this performance is in very good agreement with the prediction of the tsunami benchmark procedure we implemented (see Figures 6 and 7 for waves with this amplitude, 4.2 cm, and period, 1860 s).

In this case, the TDA configuration used was 37 tide coefficients, retrieved from 1 year bottom pressure data, and a 1 Hz sampling rate, 4000 points, 240–7200 s Hann window band-pass filter.

The postprocessing analysis of the data, which allows the accurate estimation of the tsunami wave characteristics, is shown in the bottom plot of Figure 8. Toward this end, we used a 1 Hz, 4000 points, 120–6400 Hann window applied to the detided data. The blue line in the bottom plot displays the postprocessing detided and band-passed data, visualizing the tsunami, which at this location has a period of about 1860 s and an amplitude of about 4.2 cm. The postprocessing analysis shows that the 2012 Haida-Gwaii tsunami exceed the 3 cm prescribed warning threshold at the Bullseye site at 04:04:15 UTC, i.e., 26 s before being detected by the TDA. The filtering procedure performed by the TDA slightly attenuates the true tsunami amplitude by an amount equal to 1.5 mm.

To complete the test with ONC Neptune Observatory data, we ran the TDA algorithm using a 1 min sapling rate data set acquired by Bullseye ODP889BPR from 1 December 2011 to 30 April 2012 to estimate the TDA false-alarm rate for a threshold of 3 cm, obtaining no false alarm over 5 months of data (see supporting information Figures from S16 to S19 for details).

6. Conclusions

A new real-time tsunami detection algorithm for bottom pressure data particularly suited for a very early warning framework, the TDA, has been presented and discussed. The TDA is able to detect parent tsunami signals in the tsunami frequency band with great reliability, high detection probability and very short detection delays, achieving very good performance, with a 40% of tsunamis detected within their first quarter of period and all the others within their half period. The TDA succeeds in improving the tsunami detection performances compared to other algorithms, and it is able to double the detection probability and to quadruple the number of tsunamis detected within the first quarter of period with respect to the Mofjeld algorithm. Moreover, TDA presents a lower rate of false alarms.

The new algorithm was implemented following a modular design to allow easy adaptation to different operational conditions and integration of possible further improvements. Particular care was devoted to the algorithm optimization to obtain low computational requirements, in order to enhance the TDA efficiency and enable its installation onboard low-power stand-alone devices. The TDA was implemented and tested in three long-term missions in the North East Atlantic Ocean and the Mediterranean. In the Atlantic missions, the TDA was installed onboard the GEOSTAR multidisciplinary stand-alone abyssal observatory, which was the core component of a Tsunami Early Warning System prototype developed and deployed within the framework of the NEAREST EC project. GEOSTAR operated in the Gulf of Cadiz and was connected to a land station in near real time by a two-way acoustic link from the

bottom to a surface buoy and then by a satellite link from the buoy to the shore station [*Monna et al.*, 2014].

The same algorithm was later installed onshore for the NEMO-SN1 cabled seafloor observatory deployed offshore Catania in the Ionian Sea. The connection with the shore station is through a Junction box and electro-optical cable [*Chierici et al.*, 2012; *Favali et al.*, 2013]. For both the sites, we have fixed the detection threshold at 3 cm. During these test campaigns, no parent tsunami signal exceeding the threshold was generated and the TDA has worked properly without producing any false alarms. In conclusion the TDA has been able to operate over 29 months in different sites and environmental condition without producing any false detection and when applied to Bullseye BPR data, the algorithm efficiently detected the Haida-Gwaii 2012 tsunami. Thus, we can conclude that the algorithm has been successfully tested in real contexts.

To quantitatively estimate the main features of any tsunami detection algorithm based on a threshold trigger, we developed a new testing procedure based on Monte Carlo simulation. Tsunami detection probability P and detection delay D were computed as a function of tsunami period and amplitude, as well as the false-alarm rate F. The testing procedure was found useful for evaluating the performance of tsunami detection algorithms under different operational conditions at different deployment sites.

Acknowledgments
We acknowledge financial support from EC NEAREST project (GOCE 0307110) and LIDO - EC-ESONET DM Mission (036851) and RITMARE. Some of the data used in this work (Figure 8 and supporting information Figures S1, S2, S3, S4) where kindly provided by Ocean Networks Canada; data set GEOS is available from the website http://www.moist.it/sites/iberian_margin/1/LIDO1/pressure_gauge/19; the data from DART station D125 and D165 were obtained from National Oceanic and Atmospheric Administration (2005): Deep-Ocean Assessment and Reporting of Tsunamis (DART(R)). National Geophysical Data Centre, NOAA. doi:10.7289/V5F18WNS [access date: 20/11/2015]. We acknowledge P. Favali for the critical reading of the manuscript and S. Monna for the useful suggestions.

References

Abdolali A., C. Cecioni, G. Bellotti, and J. T. Kirby (2015), Hydro-acoustic and tsunami waves generated by the 2012 HaidaGwaii earthquake: Modeling and in situ measurements, *J. Geophys. Res. Oceans*, *120*, 958–971, doi:10.1002/2014JC010385.

An, C., and P. L.-F. Liu (2014), Characteristics of leading tsunami waves generated in three recent tsunami events, *J. Earthquake Tsunami*, *8*, 1440001. doi:10.1142/S1793431114400016.

Bagheri, A., S. Greenhalgh, A. Khojasteh, M. Rahimian, and R. Attarnejad (2016), Tsunami generation and associated waves in the water column and seabed due to an asymmetric earthquake motion within an anisotropic substratum, *J. Geophys. Res. Oceans*, *121*, 7701–7715, doi:10.1002/2016JC011944.

Beltrami, G. M. (2008), An ANN algorithm for automatic, real-time tsunami detection in deep-sea level measurements, *Ocean Eng.*, *35*, 572–587.

Beltrami, G. M., and P. De Girolamo (2006), Preannuncio di un evento di maremoto—parte 1: Identificazione in tempo reale dell'evento (Tsunami Detection) Atti del XXX Convegno di Idraulica e Costruzioni Idrauliche—IDRA 2006. [Available at www.idra2006.it/referee/les/L238.pdf.]

Beltrami, G. M., and M. Di Risio (2011), Algorithms for automatic, real-time tsunami detection in wind-wave measurements. Part I: Implementation strategies and basic tests, *Coastal Eng.*, *58*, 1062–1071, doi:10.1016/j.coastaleng.2011.06.004.

Bressan, L., and S. Tinti (2011), Structure and performance of a real-time algorithm to detect tsunami or tsunami-like alert conditions based on sea-level records analysis, *Nat. Hazards Earth Syst. Sci.*, *11*, 1499–1521.

Bressan, L., and S. Tinti (2012), Detecting the 11 March 2011 Tohoku tsunami arrival on sea-level records in the Pacific Ocean: Application and performance of the Tsunami Early Detection Algorithm (TEDA), *Nat. Hazards Earth Syst. Sci.*, *12*, 1583–1606.

Bryant, E. (2014), *Tsunami The Underrated Hazard*, 3rd ed., chap. 2, Springer Int. Publ., Switzerland, doi:10.1007/978-3-319-06133-7.

Cassidy, J. F., G. C. Rogers, and R. D. Hyndman (2014), An overview of the 28 October 2012 Mw 7.7 Earthquake in Haida-Gwaii, Canada: A tsunamigenic thrust event along a predominantly strike-slip margin, *Pure Appl. Geophys.*, *171*(12), 3457–3465, doi:10.1007/s00024-014-0775-1.

Chierici, F., et al. (2007), An innovative tsunami detector operating in tsunami generation environment, *Eos Trans. AGU*, *88*(52), Fall Meet. Suppl., Abstract S53A-1031.

Chierici, F., D. Embriaco, L. Pignagnoli, L. Beranzoli, P. Favali, G. Marinaro, S. Monna, F. Bruni, F. Furlan, and F. Gasparoni (2008), An innovative tsunami detector operating on a multiparameter seafloor observatory, *Geophys. Res. Abstr.*, *10*, EGU2008-A-07393, Abstract of the contributions of the EGU General assembly Vienna, 13–18 April 2008.

Chierici, F., L. Pignagnoli, and D. Embriaco (2010), Modeling of the hydro-acoustic signal and tsunami wave generated by sea floor motion including a porous seabed, *J. Geophys. Res.*, *115*, C03015, doi:10.1029/2009JC005522.

Chierici, F., et al. (2012), NEMO-SN1 (Western Ionian Sea, off eastern Sicily): A cabled abyssal observatory with tsunami early warning capability, in *Proceedings of the International Offshore and Polar Engineering Conference 2012*, edited by S. Jin et al. 130–137, International Society of Offshore and Polar Engineers, Cupertino, Calif.

Di Risio, M., and G. M. Beltrami (2014), Algorithms for automatic, real-time tsunami detection in wind-wave measurements: Using strategies and practical aspects, *Procedia Eng.*, *70*, 545–554, doi:10.1016/j.proeng.2014.02.060.

Favali P., et al. (2013), NEMO-SN1 abyssal cabled observatory in the Western Ionian Sea, *IEEE J. Oceanic Eng.*, *38*(2), 358/374, doi:10.1109/JOE.2012.2224536.

Filloux, J. H. (1980), Pressure fluctuations on the open ocean floor over a broad frequency range: New program and early results, *J. Phys. Oceanogr.*, *10*, 1959–1971.

Filloux, J. H. (1982), Tsunami recorded on the open ocean floor, *J. Phys. Oceanogr.*, *13*, 783–796.

Filloux, J. H. (1983), Pressure fluctuations on the open ocean floor of the Gulf of California: Tides, earthquakes, tsunamis, *Geophys. Res. Lett.*, *9*, 25–28.

Foreman, M. G. G. (1977), Manual for tidal heights analysis and prediction [2004 revision], *Pac. Mar. Sci. Rep. 77-10*, Inst. of Ocean Sci., 58 pp., Patricia Bay, Sidney, B. C.

Giovanetti, G., et al. (2016), Observing volcanoes from the seafloor in the Central Mediterranean Area, *Remote Sens.*, *8*(4), 298, doi:10.3390/RS8040298.

Gonzalez, F. J., H. M. Milburn, E. N. Bernard, and J. C. Newman (1998), Deep-ocean Assessment and Reporting of Tsunamis (DART): Brief overview and status report, in *Proceedings of the International Workshop on Tsunami Disaster Mitigation*, pp. 118–129, Meteorological Agency and Science and Technology Agency, Tokyo, Japan.

Gualtieri, L., E. Stutzmann, Y. Capdeville, V. Farra, A. Mangeney, and A. Morelli (2015), On the shaping factors of the secondary microseismic wavefield, *J. Geophys. Res. Solid Earth*, *120*, 6241–6262, doi:10.1002/2015JB012157.

Kadri, U., and T. R. Akylas (2016), On resonant triad interactions of acoustic-gravity waves, *J. Fluid Mech.*, *788*, R1, doi:10.1017/jfm.2015.721.

Kibblewhite, A. C., and K. C. Ewans (1985), Wave-wave interactions, microseisms, and infrasonic ambient noise in the ocean, *J. Acoust. Soc. Am.*, *78*, 981–994.

Jay, D. A., and E. P. Flinchem (1999), A comparison of methods for analysis of tidal records containing multi-scale non-tidal background energy, *Cont. Shelf Res.*, *19*, 1695–1732.

Lamb H. (1932), *Hydrodynamics*, Dover, New York, ISBN: 0486602567.

Madsen, P. A., D. R. Fuhrman, and H. A. Schäffer (2008). On the solitary wave paradigm for tsunamis, *J. Geophys. Res.*, *113*, C12012, doi: 10.1029/2008JC004932.

McGehee, D., and J. McKinney (1997), Tsunami detection and warning capability using near shore submerged pressure transducers—Case study of the 4 October 1994 Shikotan Tsunami, in *Perspectives on Tsunami Hazard Reduction. Observation, Theory and Planning*, edited by G. Hebenstreit, pp. 133–144, Springer, Netherlands.

Meinig, C., S. E. Stalin, A. I. Nakamura, F. J. Gonzalez, and H. G. Milburn (2005), Technology developments in real-time tsunami measuring, monitoring and forecasting, in *Oceans 2005 MTS/IEEE*, September 18-23, Editor and Pubblisher Marine Technology Society, Washington, D. C.

Menold, P. H., R. K. Pearson, and F. AllgÄOwer (1999), Online outlier detection and removal, in *Proceedings of the 7th Mediterranean Conference on Control and Automation, MED'99*, Haifa, Israel, pp. 1110–1133.

Metropolis, N., and S. Ulam (1949), The Monte Carlo method, *J. Am. Stat. Assoc.*, *44*(247), 335–341, doi:10.2307/2280232.

Milburn, H. M., A .I. Nakamura, and F. J. Gonzalez (1996), Real-time tsunami reporting from deep ocean, in Proceedings of the OCEAN96 MTS/IEEE International Conference, edited by Marine Technology Society and Institute of Electrical and Electronics Engineers, pp. 390–394, Publisher Oceans '96 MTS/IEEE Conference Committee, Fort Lauderdale, Fla.

Mofjeld, H. O. (1997), Tsunami Detection Algorithm, Not published paper. [Available at http://nctr.pmel.noaa.gov/tda_documentation.html.]

Monna, S., et al. (2014), Underwater geophysical monitoring for European Multidisciplinary Seafloor and water column Observatories, *J. Mar. Syst.*, *130*, 12–30, doi:10.1016/j.jmarsys.2013.09.010.

Oliveira, T. C. A., and U. Kadri (2016), Pressure field induced in the water column by acoustic-gravity waves generated from sea bottom motion, *J. Geophys. Res. Oceans*, *120*, 958–971, doi:10.1002/2016JC011742.

Panizzo A., G. Bellotti, and P. De Girolamo (2002), Application of wavelet transform analysis to landslide generated waves, *Coastal Eng.*, *44*(4), 321–338.

Panizzo A., P. De Girolamo, and A. Petaccia (2005), Forecasting impulse waves generated by subaerial landslides, *J. Geophys. Res.*, *110*, C12025, doi:10.1029/2004JC002778.

Pawlowicz, R., B. Beardsley, and S. Lentz (2002), Classical tidal harmonic analysis including error estimates in MATLAB using T_TIDE, *Comput. Geosci.*, *28*, 929–937.

Pugh, D. T. (1982), A comparison of recent and historical tides and mean sea-levels of Ireland, *Geophys. J. R. Astron. Soc.*, *71*, 809–815.

Rabinovich, A., and M. Eblé (2015), Deep-ocean measurements of tsunami waves, *Pure Appl. Geophys.*, *172*, 3281–3312, doi:10.1007/s00024-015-1058-1.

Sanderson, K. (2008), Seismic stations could help catch tsunami waves, *Nature*, doi:10.1038/news.2008.618.

Tadepalli, S., and C. E. Synolakis (1996), Model for the leading waves of tsunamis, *Phys. Rev. Lett.*, *77*, 2141–2145.

Tanioka, Y., L. Ruff, and K. Satake (1995), The Great Kurile earthquake of October 4, 1994 tore and slab, *Geophys. Res. Lett.*, *22*(13), 1661–1664.

Tian, Y., and M. H. Ritzwoller (2015), Directionality of ambient noise on the Juan de Fuca plate: Implications for source locations of the primary and secondary microseisms, *Geophys. J. Int.*, *201*(1), 429–443, doi:10.1093/gji/ggv024.

Titov, V. V., A. B. Rabinovich, H. O. Mofjeld, R. E. Thomson, and F. J. Gonzalez (2005), The global reach of the 26 December 2004 Sumatra Tsunami, *Science*, *309*(5743), 2045–2048.

Tolkova, E. (2010), EOF analysis of a time series with application to tsunami detection, *Dyn. Atmos. Oceans*, *50*(1), 35–54.

Traer, J., and P. Gerstoft (2014), A unified theory of microseisms and hum, *J. Geophys. Res. Solid Earth*, *119*, 3317–3339, doi:10.1002/2013JB010504.

Wah, B. W., and M. Qian (2002), Constrained formulations and algorithms for stock-price predictions using recurrent FIR neural networks, in *Proceedings of the 18*th *National Conference on artificial intelligence (AAAI-2002)*, Edmonton, Alberta, Canada edited by R. Dechter, M. Kearns, and R. Sutton, The AAAI Press, Menlo Park, Calif.

Zielinski, A., and N. K. Saxena (1983), Tsunami detectability using open-ocean bottom pressure fluctuations, *IEEE J. Oceanic Eng.*, *8*(4), 272–280.